

Second harmonic generation in microdomain gratings fabricated in strontium-barium niobate crystals with an atomic force microscope

L. V. Simagina, E. D. Mishina, S. V. Semin, N. A. Ilyin, T. R. Volk et al.

Citation: *J. Appl. Phys.* **110**, 052015 (2011); doi: 10.1063/1.3624800

View online: <http://dx.doi.org/10.1063/1.3624800>

View Table of Contents: <http://jap.aip.org/resource/1/JAPIAU/v110/i5>

Published by the [American Institute of Physics](#).

Related Articles

Sub-wavelength surface gratings for light redirection in transparent substrates

Appl. Phys. Lett. **101**, 043109 (2012)

Efficient directional beaming from small apertures using surface-plasmon diffraction gratings

Appl. Phys. Lett. **101**, 041102 (2012)

Highly efficient twisted nematic liquid crystal polarization gratings achieved by microrubbing

Appl. Phys. Lett. **101**, 041107 (2012)

Divertor electron temperature and impurity diffusion measurements with a spectrally resolved imaging radiometer

Rev. Sci. Instrum. **83**, 10D521 (2012)

Fast switchable grating based on orthogonal photo alignments of ferroelectric liquid crystals

Appl. Phys. Lett. **101**, 031112 (2012)

Additional information on J. Appl. Phys.

Journal Homepage: <http://jap.aip.org/>

Journal Information: http://jap.aip.org/about/about_the_journal

Top downloads: http://jap.aip.org/features/most_downloaded

Information for Authors: <http://jap.aip.org/authors>

ADVERTISEMENT



Special Topic Section:
PHYSICS OF CANCER

Why cancer? Why physics? [View Articles Now](#)

Second harmonic generation in microdomain gratings fabricated in strontium-barium niobate crystals with an atomic force microscope

L. V. Simagina,¹ E. D. Mishina,² S. V. Semin,² N. A. Ilyin,² T. R. Volk,^{1,a)} R. V. Gainutdinov,¹ and L. I. Ivleva³

¹*Shubnikov Institute of Crystallography of the Russian Academy of Sciences, 119333 Moscow*

²*Moscow State Institute of Radio Engineering, Electronics and Automation, 119454 Moscow*

³*Prokhorov General Physics Institute of the Russian Academy of Sciences, 119991 Moscow*

(Received 17 February 2011; accepted 11 June 2011; published online 2 September 2011)

Regular surface domain gratings were created in strontium barium niobate crystals by local poling with an AFM-tip. Piezoresponse force microscopy was utilized to subsequently image the domain patterns and to investigate their temporal and thermal stability. The gratings were examined by means of nonlinear diffraction in reflection geometry using a Ti-sapphire laser (800 nm) as pump source. The well-resolved second harmonic diffraction patterns were recorded for various angles of incidence of the fundamental wave. The origin of the observed nonlinear diffraction is discussed.

© 2011 American Institute of Physics. [doi:10.1063/1.3624800]

I. INTRODUCTION

In this paper we present first observations of second harmonic generation (SHG) in surface microdomain gratings recorded in $\text{Sr}_x\text{Ba}_{1-x}\text{Nb}_2\text{O}_6$ (SBN-x) crystals locally applying a dc-voltage with the help of the tip of an atomic force microscope (AFM). The optical experiments were performed using nonlinear diffraction. The investigations are motivated by the prospects of 1D- and 2D- ferroelectric domain patterns for optical-frequency conversion using quasi-phase matching (QPM). Numerous publications, reviews, and monographs cover this subject (see, e.g., Refs. 1 and 2). At present, in particular 2D arrays have attracted increasing attention in view of their applicability as nonlinear photonic crystals.³ As it is known, one of the most promising methods for the creation of microdomain arrays in ferroelectrics uses local poling with the help of an AFM tip.⁴ Recently, we have demonstrated the creation of various types of rather stable 1D- and 2D- regular microdomain arrays, as well as more complex 2D structures in strontium barium niobate (SBN) by applying dc-voltages of less than 10 V to the AFM tip.⁵⁻⁷ But also for nonlinear-optical applications SBN is an attractive material since in addition to the high nonlinear quadratic permittivity $\chi^{(2)}$ (Ref. 8), it shows the unique effect of stochastic (broadband) optical frequency conversion in a disordered domain configuration (see, e.g., Refs. 9 and 10, and Refs. therein). All these properties make of SBN a promising material for the investigation of parametric nonlinear-optical phenomena using domain arrays. The main aim of the present work was to investigate the potential of AFM-written microdomain gratings in SBN for optical frequency conversion.

II. EXPERIMENT

For our investigations were used congruent SBN-0.61 crystals grown by a modified Stepanov's technique.¹¹ The

samples were optically polished, 0.13 – 0.3 mm thick z-cut plates. All experiments were performed in polydomain crystals. In order to assure for identical initial conditions, prior to the domain recording the samples were annealed at $T > T_c \approx 83^\circ\text{C}$ (where T_c corresponds to the peak of $\varepsilon(T)$ measured at 1 kHz).

The AFM experiments were carried out with an NTEGRA PRIMA AFM (NT-MDT, Moscow) operated in contact mode. The domain configuration was recorded simultaneously to the topography by piezoresponse force microscopy (PFM) using Si probes with a conductive Ti/Pt coating (CSC21, MikroMasch, Estonia). The probes had a tip radius of $R \leq 40$ nm, cantilever stiffness of $k \sim 0.12$ N/m (A cantilever) and $k \sim 2.0$ N/m (B cantilever), and resonance frequencies of $f \sim 12$ kHz (A cantilever) and $f \sim 105$ kHz (B cantilever). A more detailed description of our AFM equipment and our experimental methods can be found in Refs. 5-7. Local poling of the sample was performed by applying a dc-voltage U_{DC} to the conductive probe while the tip was in contact with the crystal surface. A conducting carbon adhesive tape was used as back electrode which as a result fastened the sample to a standard wafer grounded with the help of a spring contact.

In this paper, we present our results obtained on regular microdomain arrays which are in the form of domain stripes of opposite polarity (Fig. 1), normal to the sample surface. So far, we have not estimated the depth of the domains created, however, according to some indirect estimates they are shallow (≤ 10 μm). The gratings were recorded using a raster lithography method based on a graphic template. Therefore, the tip was displaced point-by-point along two orthogonal coordinates and at every point a voltage pulse ($U_{DC} = \pm 50$ V and $t_p = 7$ ms) was applied to it. The distance between the individual points was set to $\Delta \sim 50$ nm since at this distance adjacent domains (merge) overlap, as shown previously.⁵⁻⁷ After domain writing the area was scanned by PFM for confirming the created domain pattern. When scanning the surface

^{a)}Electronic mail: volk@ns.crys.ras.ru.

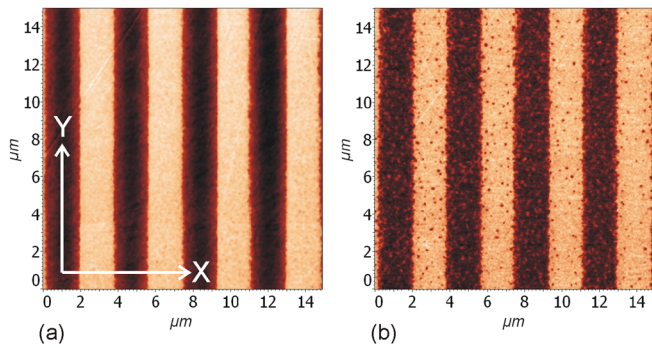


FIG. 1. (Color online) PFM images of an AFM-written domain grating 5 mins (a) and three months (b) after recording. The grating period is $\Lambda = 3.6 \mu\text{m}$. (The light and dark areas represent “positive” and “negative” domain stripes).

by PFM the electromechanical response H_ω was measured following the procedure described in Ref. 12. Note that the scan lines of H_ω qualitatively characterize the spatial distribution of $\chi^{(2)}$.

The microdomain gratings were written in an area of about $80 \times 80 \mu\text{m}^2$. These tiny dimensions impede the focusing of the pumping wave on the domain array only. Indeed, any unwanted irradiation of the surrounding area would adulterate the results. In order to overcome this problem highly reflecting, 20 nm thick chromium frames, $200 \times 200 \mu\text{m}^2$ in size and $60 \mu\text{m}$ bar width, were coated on the sample surface by photolithographic means. The microdomain gratings were recorded inside these frames (see below).

The gratings were examined by nonlinear diffraction as it was proposed in Ref. 13. Since the gratings were written in initially polydomain crystals, we used reflection geometry for our investigations. As mentioned above, random bulk domains lead to strong, diffuse SHG (Refs. 9 and 10). Consequently, using transmission geometry, the SHG signal diffracted by the shallow microdomain grating would possibly not be detectable due to the background of the bulk SH emission. Figure 2 illustrates the experimental setup used. Pumping was realized by a Ti-sapphire laser with a wavelength of 800 nm and a repetition rate of 82 MHz, the pulse average power and duration were 5–30 mW and 100 fs, respectively. The fundamental beam, polarized in the incidence plane (p -polarization), was focused onto the sample with a minimum waist of about $100 \mu\text{m}$ (Fig. 2, inset). The reflected p -polarized SH wave was detected by the photomultiplier tube (PMT in Fig. 2) mounted on a rotation stage. To obtain the angular dependence of the diffracted SH signal, the PMT was rotated by up to $\pm 30^\circ$ with the sample as the pivot point. The sample itself was mounted on a goniometer which provided the possibility of rotating the sample and thus varying the angle of incidence θ_i of the pump wave between 30° and 60° . Additionally, the goniometer provided a translation of the sample along the X and Y -axes. Thus, this experimental setup permits to obtain the angular dependency of the SH signal for various angles of incidence θ_i generated at the very same location of the microdomain grating (see Fig. 2, inset).

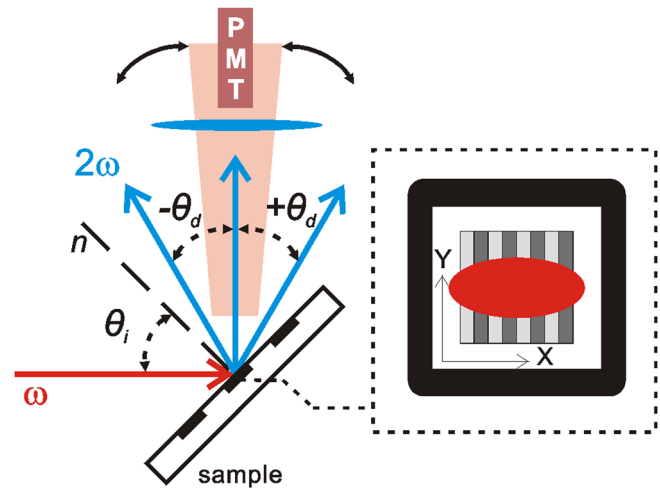


FIG. 2. (Color online) (a) Setup of the optical experiment. Solid arrows indicate angular movement of the detection arm with PMT. ω and 2ω denote the fundamental and SH waves, respectively; θ_i and θ_d are the angles of incidence and diffraction, respectively. Three microdomain gratings recorded in the sample are depicted by the black. (b) The zoomed schematic view of a single grating within the metal frame; the red ellipse depicts the laser spot whose elliptical shape is due to an oblique incidence of the fundamental beam.

III. EXPERIMENTAL RESULTS AND DISCUSSION

A. Characterization of the domain gratings

Striped microdomain gratings with spatial periods ranging from 2 to $4 \mu\text{m}$ were recorded. The width of every domain stripe is of about half the period Λ of the grating (Fig. 1). The boundaries between antiparallel domains are smeared out by 70 nm. Such diffuse domain boundaries are characteristic for the relaxor ferroelectric SBN (Ref. 14). No topographical relief could be detected at the domain boundary, so unlike in LiNbO_3 (Ref. 15) no mechanical stress exist in these regions.

We first describe the temporal evolution of the recorded gratings on the basis of an example with $\Lambda = 3.6 \mu\text{m}$ (Fig. 1). Figure 3(a) shows two scanlines extracted from Figs. 1(a) and 1(b). Obviously after three months, the amplitude of the grating has decreased to 20% of its initial value. Figure 3(b) shows the relaxation of the electromechanical signal amplitude on a shorter scale of eight days. As can be seen, after a noticeable decay during relatively short time of few hours only, the contrast remains practically stable. Indeed, some samples show at longer relaxation times the emergence of nanoscaled domains, seen in Fig. 1(b) as dark spots in the area of the bright stripes and vice versa (bright spots in the dark stripes). Obviously the domain structure tends toward a polydomain state which is driven by the underlying random bulk domain structure. Meanwhile, the amplitudes of the scanlines of the images are decaying very slowly.

In addition to a relatively high persistence the recorded gratings show sufficient temperature stability. The result of thermal annealing of the sample is illustrated in Fig. 4. The sample was heated to a certain temperature T , hold at this temperature for 90 min and cooled down to room temperature. After annealing, the depolarized area ΔS of the initially

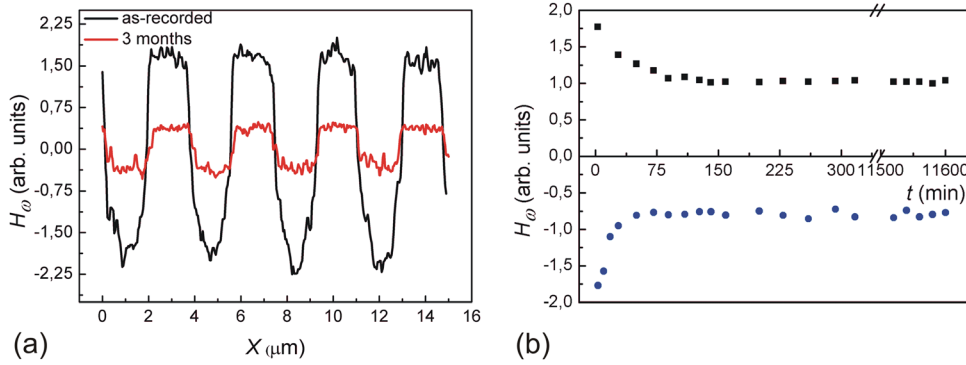


FIG. 3. (Color online) (a) Scanlines of the images shown in Fig. 1; 5 mins (black) and three months (red) after recording the grating. (b) Temporal decay of the grating: upper and lower curves present the relaxation of the positive and negative, i.e., bright and dark domain stripes in Fig. 1.

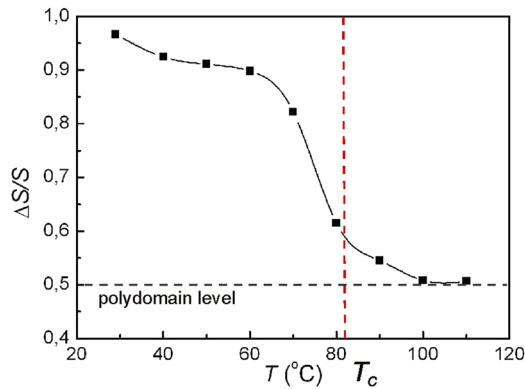


FIG. 4. (Color online) Thermal annealing of the domain grating (T_c is the phase transition temperature).

positive, i.e., the bright area in Fig. 1 was estimated. Figure 4 presents the degree of polarization $\Delta S/S$ (where S is the total area of the positive domain stripes before annealing) versus the annealing temperatures T . As it can be seen from the graph in Fig. 4, the grating partially persists even after annealing close to T_c .

B. Nonlinear-optical diffraction

Figure 5(a) presents the angular dependence of the reflected SH on the angle of incidence θ_i . When the fundamental wave is incident to the grating, the patterns measured for all θ_i show a central peak and two asymmetrical side peaks [curves 1 – 3 in Fig. 5(a)]. The asymmetry increases with increasing θ_i . Both, the central and side peaks stand out against a significant background and can be well resolved for the total range of detection angles. In the case the fundamen-

tal wave is incident in an area not comprising a microdomain grating, the reflected pattern reveals the central peak only [curve 4 in Fig. 5(a)]. Consequently, the side peaks are caused by the diffraction of the SH at the grating. In spite of the fact that the microdomain grating is very shallow, the diffraction patterns are very well resolved. Interestingly, the temporal dependence of the side peak intensities is governed by the contrast [Fig. 3(a)] and only weakly sensitive to the abovementioned partial polydomainization of the domain stripes. Figure 5(b) presents the diffraction angles of the “right” and “left” side peaks versus the angle of incidence θ_i . With increasing θ_i the diffraction angles slightly increase.

We now discuss the structure of the reflected patterns [Fig. 5(a)] starting from the origin of the side peaks

As known, the nonlinear Bragg diffraction from a regular $\chi^{(2)}$ grating is obtained at a specific angle between the fundamental and SH waves provided that the vectorial phase matching is satisfied

$$\vec{k}_{2\omega} = 2\vec{k}_\omega + m\vec{Q} \quad (1)$$

where \vec{k}_ω and $\vec{k}_{2\omega}$ are the wave vectors of the fundamental and SH waves, respectively, and $\vec{Q} = 2\pi/\Lambda$ is the reciprocal grating vector, $m = \pm 1, \pm 2, \dots$

Nonlinear Bragg diffraction from regular domain structures as well as non-collinear SHG under QPM conditions with an oblique beam incidence on the domain grating were repeatedly reported in various ferroelectric crystals (see, e.g., Refs. 16–19). The nonlinear Raman-Nath diffraction was recently observed in thin domain gratings (see Ref. 20, and Refs. therein). In contrast to the listed publications, the results presented in our work were obtained in reflection geometry under non-normal incidence. In order to achieve

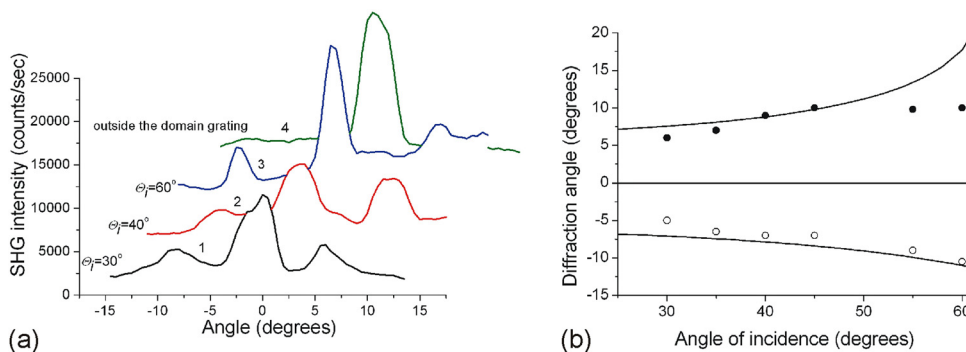


FIG. 5. (Color online) (a) The angular dependencies of the SHG intensity for different angles of incidence; the curve 4 is obtained when the fundamental beam is incident onto the crystal outside of the domain grating. (b) The diffraction angles of the “right” and “left” peaks as a function of the angle of incidence; the solid curves present fits using Eq. (2).

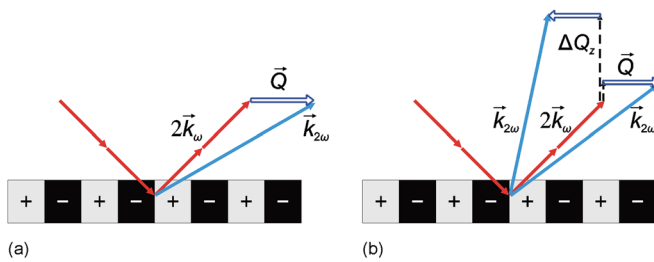


FIG. 6. (Color online) The scheme of the wave-vector (photon momentum) conservation for the cases of presence (a) and absence (b) of quasi-phase matching conditions for non-normal incidence.

QPM in reflection geometry, condition, Eq. (1), has to be satisfied according to the vectorial scheme shown in Fig. 6(a).

Our estimates, however, show that in SBN crystals exhibiting very high refractive indices [$n(\omega) = 2.246$, $n(2\omega) = 2.452$ for p -polarized waves⁸] the QPM condition, Eq. (1), might be fulfilled for $m = 8$ only in the non-collinear geometry for grating periods of about $\Lambda \sim 3.62 - 3.68 \mu\text{m}$. For $m = 1$ satisfying condition, Eq. (1), would require very small periods of about $\Lambda \sim 0.405 - 0.485 \mu\text{m}$. In any case the angle of incidence should be smaller than 10° , since for higher θ_i total internal reflection would make a measurement of the diffracted SH impossible. Summing up, the used experimental conditions do not permit to satisfy Eq. (1) in the non-collinear geometry under non-normal incidence. The observed nonlinear diffraction [Fig. 5(a)] must therefore be related to another origin.

Apart from the QPM condition, Eq. (1), nonlinear diffraction can occur due to the regular modulation of the nonlinear susceptibility, when the grating itself is involved in the wave-vector conservation law [Fig. 6(b)]. Analogously to Raman-Nath linear diffraction, nonlinear diffraction of this type is based on the fact that the grating acts as an infinite mass where the photon meets a perfectly inelastic collision. In such an event the excess momentum of the z -component ΔQ_z [Fig. 6(b)] is transferred to the grating.

A general expression for the SH luminous flux in the case of nonlinear diffraction was deduced in the landmark work of Ref. 13 [Eq. (3), therein]. When the law of momentum conservation is considered for the in-plane direction only, the third term of Eq. (3) in Ref. 13 gives for our case the following expression for the intensity distribution and the diffraction angle maxima positions:

$$\Lambda(\sin \theta_i - \sin \theta'_d) = \pm m \lambda_{2\omega}, \quad (2)$$

(where θ'_d is the diffraction relative to the normal)

In Fig. 5(b), the solid curves show fits to the experimental data using Eq. (2). The grating period Λ estimated from these curves is in very good agreement with the PFM measurement (Fig. 1). This result supports the proposed interpretation of the origin of SHG diffraction peaks.

The described type of the nonlinear diffraction differs from that under the QPM conditions in the same manner as the non-Bragg linear diffraction differs from the Bragg one. The former can be observed for any angle of incidence, because ΔQ_z allows for a continuous set of values. The latter requires the fulfillment of Eq. (1) for the discrete set of val-

ues $\pm m$, i.e., it can occur only for certain angles of incidence.

The central peak observed within and beyond the gratings [curves 1–3 and 4, respectively, in Fig. 5(a)] originates from the specular nonlinear reflection at a depth equal to the coherence length. It exists at any interface and may arise from various sources [dipoles, quadrupoles, etc. (Refs. 21 and 22)]. Additionally, it may be caused by a certain asymmetry of the grating. As seen from Fig. 3(b), the positive and negative domain stripes are decaying differently. Therefore, with time the grating becomes slightly asymmetrical.

A large non-structured background emerging in all patterns is obviously due to the broadband SHG in the disordered domain structure^{9,10} beneath the grating.

One may perceive a fundamental difference between our results on the nonlinear diffraction from those observed in periodically-poled LiNbO₃ at an oblique beam incidence.¹⁷ In LiNbO₃, significant mechanical stress and/or a space-charge field at the domain boundary lead to a change of the refractive indices via the piezo-optical and/or electro-optical effects.¹⁵ As a consequence, serial domain boundaries results in a refractive index grating. Due to this effect, the authors of Ref. 17 detected the coexistence of linear and nonlinear diffraction gratings within the periodical domain structure. In contrast to this, as mentioned above, no mechanical stress exists at the domain boundaries in SBN, so this domain grating provides no linear diffraction.

IV. CONCLUSION

Using standard AFM-writing of domains by applying dc-voltages to the tip we recorded ferroelectric domain patterns in thin surface layers of SBN polydomain crystals. These striped microdomain arrays had spatial periods in the range from 2 to 4 μm exhibiting rather high temporal and thermal stability. The recorded domain arrays were investigated by their ability to act as nonlinear-optical diffraction gratings. In spite of a very high ratio of the crystal thickness to the grating thickness, using reflection geometry a rather high contrast of the diffraction patterns of the Raman-Nath type could be obtained. The results obtained recommend SBN crystals as a convenient laboratory medium for studies of optical frequency conversion in microdomain ensembles of specified design.

ACKNOWLEDGMENTS

This work was supported by the Russian Foundation for Basic Researches (Project Nos. 09-02-00969a and 11-02-00888a), by the Branch of Physical Sciences, Russian Academy of Sciences (program “Fundamental Problems of Photonics and Physics of New Optical Materials”) and by the Russian Ministry of Education and Science (the Program “Cadres”). Useful discussions with M. V. Gorkunov and A. I. Morozov and very important corrections introduced by E. Soergel are highly appreciated.

¹M. M. Fejer, G. A. Magel, D. H. Jundt, and R. L. Byer, *IEEE J. Quantum Electron.* **28**, 2631 (1992).

²D. S. Hum and M. M. Fejer, *Comptes Rend.* **8**, 180 (2007).

³V. Berger, *Phys. Rev. Lett.* **81**, 4136 (1998).

- ⁴A. L. Kholkin, S. V. Kalinin, A., Roelofs, and A. Gruverman, "Review of Ferroelectric Domain Imaging by Piezoresponse Force Microscopy," in *Scanning Probe Microscopy. Electrical and Electromechanical Phenomena at the Nanoscale*, S. Kalinin and A. Gruverman (Springer, New York, 2007), Vol. I, p. 173.
- ⁵R. V. Gainutdinov, T. R. Volk, O. A. Lysova, I. I. Razgonov, A. L. Tolstikhina, and L. I. Ivleva, *Appl. Phys. B*, **95**, 505 (2009).
- ⁶R. V. Gainutdinov, T. R. Volk, O. A. Lysova, A. L. Tolstikhina, and L. I. Ivleva, *JETP Lett.* **90**, 303 (2009).
- ⁷T. R. Volk, L. V. Simagina, R. V. Gainutdinov, A. L. Tolstikhina, and L. I. Ivleva, *J. Appl. Phys.* **108**, 042010 (2010).
- ⁸Yu. S. Kuz'minov, *Ferroelectric Crystals for Laser Radiation Control* (Adam Hilger, Bristol, 1990).
- ⁹S. Kawai, T. Ogawa, H. S. Lee, R. C. DeMattei, and R. S. Feigelson, *Appl. Phys. Lett.* **73**, 768 (1998).
- ¹⁰P. Molina, M. O. Ramirez, and L. E. Bausa, *Adv. Funct. Mater.* **18**, 709 (2008).
- ¹¹I. Ivleva, N. V. Bogodaev, N. M. Polozkov, and V. V. Osiko, *Opt. Mater.* **4**, 168 (1995).
- ¹²A. V. Ankudinov and A. N. Titkov, *Phys. Solid State* **47**, 1148 (2005).
- ¹³I. Freund, *Phys. Rev. Lett.* **21**, 1404 (1968).
- ¹⁴P. Lehnen, W. Kleemann, Th. Woiike, and R. Pankrath, *Phys. Rev. B*, **64**, 224109 (2001).
- ¹⁵V. Gopalan, V. Dierolf, and D. A. Scrymgeour, *Annu. Rev. Mater. Res.* **37**, 449 (2007).
- ¹⁶A. L. Aleksandrovskii and V. V. Volkov, *Quantum Electron.* **26**, 542 (1996).
- ¹⁷A. L. Aleksandrovskii, O. A. Gliko, I. I. Naumova, and V. I. Pryalkin, *Quantum Electron.* **26**, 641 (1996).
- ¹⁸S. Moscovich, A. Arie, R. Urenski, A. Agronin, G. Rosenman, and Y. Rosenwaks, *Opt. Express* **12**, 2236 (2004).
- ¹⁹A. S. Aleksandrovsky, A. M. Vyunishev, I. E. Shakhura, A. I. Zaitsev, and A. V. Zamkov, *Phys. Rev. A*, **78**, 031802 (2008).
- ²⁰S. M. Saltiel, D. N. Neshev, W. Krolikowski, A. Arie, O. Bang, and Yu. S. Kivshar, *Opt. Lett.* **34**, 848 (2009).
- ²¹P. Guyot-Sionnest and Y. R. Shen, *Phys. Rev. B*, **38**, 7985 (1988).
- ²²M. Fiebig, V. V. Pavlov, and R. V. Pisarev, *J. Opt. Soc. Am. B*, **22**, 96 (2005).